

Observation of flat-band and band transition in the synthetic space

Guangzhen Li^{1,*}, Luoia Wang^{1,*}, Rui Ye¹, Shijie Liu¹, Yuanlin Zheng^{1,2}, Luqi Yuan^{1✉}, and Xianfeng Chen^{1,2,3,4✉}

¹State Key Laboratory of Advanced Optical Communication Systems and Networks, School of Physics and Astronomy, Shanghai Jiao Tong University, Shanghai 200240, China

²Shanghai Research Center for Quantum Sciences, Shanghai 201315, China

³Jinan Institute of Quantum Technology, Jinan 250101, China

⁴Collaborative Innovation Center of Light Manipulation and Applications, Shandong Normal University, Jinan 250358, China

*These authors contribute equally to this work.

✉yuanluqi@sjtu.edu.cn; xfchen@sjtu.edu.cn

ABSTRACT

Constructions of synthetic lattices in photonics attract growingly attentions for exploring interesting physics beyond the geometric dimensionality, among which modulated ring resonator system has been proved as a powerful platform to create different kinds of connectivities between resonant modes along the synthetic frequency dimension with many theoretical proposals. Various experimental realizations are investigated in a single ring resonator, while building beyond simple synthetic lattices in multiple rings with different types remains lacking, which desires to be accomplished as an important step further. Here, we implement the experimental demonstration of generating the one-dimensional Lieb lattice along the frequency axis of light, realized in two coupled ring resonators while the larger ring undergoing dynamic modulation. Such synthetic photonic structure naturally exhibits the physics of flat band. We show that the time-resolved band structure read out from the drop-port output of the excited ring is the intensity projection of the band structure onto specific resonant mode in the synthetic momentum space, where gapless flat band, mode localization effect, and flat to non-flat band transition are observed in experiments and verified by simulations. Our work gives a direct evidence for the constructing synthetic Lieb lattice with two rings, which hence makes a solid step towards experimentally constructing more complicated lattices in multiple rings associated with synthetic frequency dimension.

Main text

Synthetic dimension in photonics attracts broad interest and experiences important experimental achievements in recent years¹⁻⁴, which shows the great capability for studying fundamental physical phenomena with exotic artificial connectivities⁵⁻⁹, manipulating light in various ways¹⁰⁻¹⁷, and pointing towards exploring higher-dimensional physics beyond three dimensions¹⁸⁻²⁰. Among these experimental achievements, different degrees of freedom of light, including arrival times of pulses^{10,11}, frequencies²¹⁻²³, and modal dimensions⁸, have been used to construct the synthetic dimension. Hence, a variety of novel physics have been demonstrated in synthetic dimensions, such as the photonic topological insulator⁸, the Hall ladder with the effective magnetic flux²⁴, the trajectory of dynamic band structures²⁵, and the topological funneling with non-Hermitian physics²⁶, whose physical models are hard to be built in structures with only spatial dimensions.

Besides different photonic platforms for constructing synthetic dimensions, dynamically modulated ring resonator system has manifested as a powerful platform where resonant modes with equally-spaced frequencies are coupled by the external modulation and then synthetic frequency dimension is created^{21,22}. The modulation applied by external voltages provides the unique advantages of breaking the constrain of fixed geometric structures after fabrication and thus provides an important possibility of achieving complicated functionalities with great experimental flexibility and reconfigurability⁴. Up to now, experimental implementations in ring resonator systems including fiber loops or on-chip microrings have demonstrated the creation of the synthetic frequency dimension in a single ring resonator^{23-25,27-30}, where versatile physical phenomena have been shown, such as measuring band structures^{23,25}, observing spectral Bloch oscillations²⁸, and generating arbitrary topological windings²⁹. On the other hand, many theoretical proposals have been explored where formations of photonic lattice with different types of rings in higher dimensions can intrigue studies of rich physics, such as simulating two-dimensional Haldane model⁷, three-dimensional topological insulator³¹, and four-dimensional quantum Hall effect²² in multiple rings. However, to realize these theoretical proposals, it requires constructing a synthetic space including the frequency dimension in two or more rings³² with perhaps different types, which are still missing in experiments, due to the fact that resonant modes circulated in each ring at different type need fully precise synchronization in order to stably connect same synthetic frequency sites in different rings. In other words, the experimental feasibility for constructing synthetic space in multiple rings with different types are questionable so far. Therefore, as a crucial step towards exploring complex lattice structures in the

synthetic space with multiple rings, one desires the demonstration of creating the synthetic space in two coupled rings with different types in the experiment.

In this work, we prove the capability for coupling two rings with different types where one ring undergoes the dynamic modulation, and observe flat-band physics in a synthetic space including the frequency dimension. Such configuration supports a one-dimensional (1D) photonic Lieb lattice but associated with synthetic frequency dimension. One intrinsic physics of such lattice is the naturally existence of the flat (dispersionless) band, which has found important applications with the localization effect^{33–37}. In our experiments, the time-resolved energy bands from the drop-port output of the excited ring are obtained, corresponding to the projection of the band structures of the 1D Lieb lattice, which, however, is on the synthetic dimension. Moreover, by exciting the resonant modes through the selected input port of one ring and recording the output transmission from the same ring, we observe the effective localization of the resonant modes near the flat band. Such flat band in the synthetic space can further be modified by adding the long-range couplings in the modulation, which leads to the transition from the flat to non-flat bands. We provide theoretical analysis, which gives excellent agreements with experiments. Our work explores the flat-band physics in a synthetic Lieb lattice along the frequency dimension by successfully synchronizing two rings with different types, which exhibits a crucial step towards the potential for experimentally constructing more complicated synthetic lattices in multiple rings.

We start with illustrating the model including two types of ring resonators composed by the waveguide or fiber loop fabricated with same materials at different lengths, labelled as A and B as shown in Fig. 1(a). In the absence of the group velocity dispersion, the ring resonator supports a set of modes with equally spaced frequencies. If we set the central resonant frequency at ω_0 , the n^{th} mode in the ring A(B) has the frequency $\omega_{A(B),n} = \omega_0 + n\Omega_{A(B)}$, where $\Omega_{A(B)} = 2\pi v_g/L_{A(B)}$ is the free spectral range (FSR) of ring A(B), and v_g is the group velocity. We consider the length of ring A (L_A) twice long as the length of ring B (L_B), i.e., $L_A = 2L_B$, which gives $2\Omega_A = \Omega_B \equiv \Omega$. There is an electro-optic modulator (EOM) placed inside the ring A with the modulation frequency $\Omega_M = \Omega/2$, the modulation strength g , and the modulation phase ϕ , which provides the connectivity between adjacent resonant modes in ring A, while there is no modulator in ring B so resonant modes in ring B remain un-connected. Two resonant modes in two rings at the same frequency can be coupled through evanescent waves or fiber coupler with the coupling strength κ [see Fig. 1(b)]. Therefore, there exist three types of modes in the system, defined as A_n , B_n , and C_n , where A_n and C_n are the resonant modes at frequencies ω_n and $\omega_n + \Omega/2$ in ring A, and B_n is the resonant mode at frequency ω_n in ring B with $\omega_n = \omega_0 + n\Omega$. In particular, modes A_n and

B_n are coupled for the same n , while A_n is coupled to C_{n-1} and C_n through the modulation under the lowest-order approximation, resulting the synthetic lattice shown in Fig. 1(b).

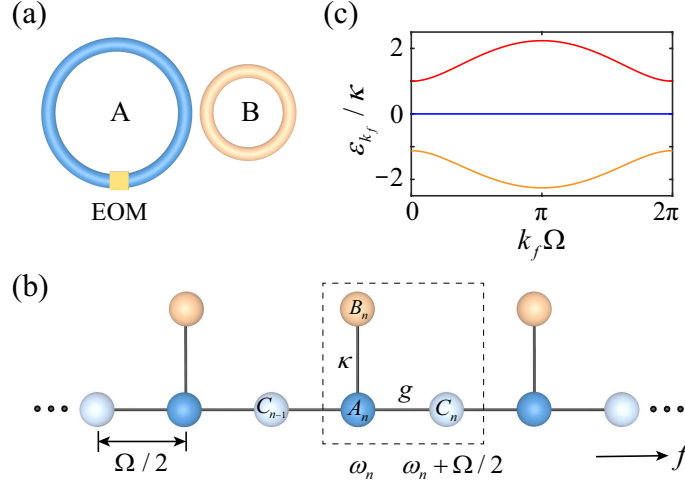


Figure 1. Configuration of a 1D synthetic photonic Lieb lattice. (a) Two coupled ring resonators, where the FSR of ring A is half of the FSR of ring B, i.e., $2\Omega_A = \Omega_B \equiv \Omega$. Ring A undergoes dynamic modulation by placing an EOM with the modulation frequency $\Omega_M = \Omega/2$. (b) The system in (a) can be mapped into a 1D photonic Lieb lattice along the synthetic frequency dimension (f), with A_n , B_n , and C_n indicating three types of lattice sites. (c) The corresponding band structures of the synthetic Lieb lattice in (b) with $g = \kappa$ and $\phi = -0.5\pi$.

The corresponding tight-binding Hamiltonian of the system is³⁸

$$\begin{aligned}
 H = H_0 + H_1 = & \sum_n \left[\omega_n \left(a_n^\dagger a_n + b_n^\dagger b_n \right) + \left(\omega_n + \Omega/2 \right) c_n^\dagger c_n \right] \\
 & + \kappa \sum_n \left(a_n^\dagger b_n + h.c. \right) + 2g \cos(\Omega t/2 + \phi) \sum_n \left(a_n^\dagger c_n + a_n^\dagger c_{n-1} + h.c. \right),
 \end{aligned} \tag{1}$$

where a_n^\dagger , b_n^\dagger , and c_n^\dagger (a_n , b_n , and c_n) are the creation (annihilation) operators for the modes A_n , B_n and C_n , respectively. H_0 denotes the first summation terms on the right of Eq. (1), referring to the unperturbed part for all resonant modes, while H_1 gives the interaction terms. Equation (1) can be simplified into the interaction picture by considering $e^{iH_0 t} H_1 e^{-iH_0 t}$, and taking the rotating-wave approximation³⁹, which results in

$$H_c = \kappa \sum_n a_n^\dagger b_n + g \sum_n \left(a_n^\dagger c_n e^{i\phi} + a_n^\dagger c_{n-1} e^{-i\phi} \right) + h.c.. \tag{2}$$

Equation (2) describes the Hamiltonian of a synthetic lattice structure, which is analog to the 1D spatial Lieb lattice^{40–42}, but it is along the frequency axis of light.

To understand the underlying physics of the Hamiltonian described in Eq. (2), we can re-write Eq. (2)

into the k_f space

$$H_k = \kappa \sum_{k_f} \left(a_{k_f}^\dagger b_{k_f} + b_{k_f}^\dagger a_{k_f} \right) + 2g \sum_{k_f} \left(a_{k_f}^\dagger c_{k_f} + c_{k_f}^\dagger a_{k_f} \right) \cos(k_f \Omega / 2 + \phi), \quad (3)$$

where k_f is the wave vector reciprocal to the frequency dimension acting as a time variable⁴. The corresponding photonic band structure of the system is then given by

$$\varepsilon_{k_f,0} = 0, \quad \varepsilon_{k_f,\pm} = \pm \sqrt{[2g \cos(k_f \Omega / 2 + \phi)]^2 + \kappa^2}, \quad (4)$$

where $\varepsilon_{k_f,j}$ ($j = 0, \pm$) are the eigenvalues from Eq. (3), corresponding to three bands plotted in Fig. 1(c) within the first Brillouin zone with $k_f \in [0, 2\pi/\Omega]$. One can see a flat band $\varepsilon_{k_f,0}$ in the middle gapped from the upper and lower dispersive bands $\varepsilon_{k_f,\pm}$, which indicates that light can be efficiently localized in the flat band without scattering^{33–37}. Let $\psi_{k_f,j} = (\psi_{k_f,j}^A, \psi_{k_f,j}^B, \psi_{k_f,j}^C)^\top$ be the eigenstates corresponding to $\varepsilon_{k_f,j}$, with $\psi_{k_f,j}^A$, $\psi_{k_f,j}^B$ and $\psi_{k_f,j}^C$ being the projection of the eigenstates on the three modes (A_k , B_k , and C_k) in the k_f space, and then we have

$$\begin{aligned} \psi_{k_f,0} &= (0, -G, \kappa)^\top / \sqrt{G^2 + \kappa^2}, \\ \psi_{k_f,\pm} &= (\pm \sqrt{G^2 + \kappa^2}, \kappa, G)^\top / \sqrt{2(\kappa^2 + G^2)}, \end{aligned} \quad (5)$$

with $G = 2g \cos(k_f \Omega / 2 + \phi)$. One notes that the flat band ($j = 0$) has no projection onto the mode A_k due to $\psi_{k_f,0}^A = 0$, while the two dispersive bands ($j = \pm$) are asymmetrically projected onto the mode A_k but symmetrically projected onto modes B_k and C_k .

To implement the idea of the 1D synthetic photonic Lieb lattice described in Eq. (2) for the potential experimental demonstration, we continue with considering a realistic model of two ring resonators coupled with input and output waveguides. In the following, we consider two excitation cases by selectively choosing the input/output ports, which are referred as B *in*→B *out* and A *in*→A *out* as sketched in the inserted figures in Fig. 2. First, we inject the field into the system through the input port of ring B and measure drop-port output of ring B as well (B *in*→B *out*), in which way only frequency mode B_n in ring B is directly excited. We consider the photon state being $|\psi\rangle = \sum_n [v_{a,n}(t)a_n^\dagger + v_{b,n}(t)b_n^\dagger + v_{c,n}(t)c_n^\dagger]|0\rangle$, where $v_{a,n}$, $v_{b,n}$, and $v_{c,n}$ are the amplitudes of the photon states of the frequency modes A_n , B_n , and C_n , respectively. By applying the Schrödinger equation $i|\dot{\psi}\rangle = H_c|\psi\rangle$ with H_c defined in Eq. (2), we obtain

the input/output coupled amplitude equations for the n^{th} modes⁴

$$\begin{aligned}\dot{v}_{a,n} &= -i\kappa v_{b,n} - ig(v_{c,n}e^{i\phi} + v_{c,n-1}e^{-i\phi}) - \gamma v_{a,n}, \\ \dot{v}_{c,n} &= -ig(v_{a,n}e^{-i\phi} + v_{a,n+1}e^{i\phi}) - \gamma v_{c,n}, \\ \dot{v}_{b,n} &= -i\kappa v_{a,n} - \gamma v_{b,n} + i\sqrt{\gamma_B} S_{\text{in}}^B e^{in\Omega t - i\Delta\omega t},\end{aligned}\quad (6)$$

where S_{in}^B is the input laser source, $\Delta\omega$ is the frequency detuning between the input field frequency and the reference frequency ω_0 , γ is the total loss, and γ_B is the coupling strength between ring B and waveguides. The amplitude of the output field at the drop-port of ring B is given by $S_{\text{out}}^B = -i\sqrt{\gamma_B} \sum_n v_{b,n} e^{-i\omega_n t}$. The normalized drop-port transmission $T_{\text{out}}^B = |S_{\text{out}}^B/S_{\text{in}}^B|^2$ can be expressed in the k_f space as [see supplementary materials]

$$T_{\text{out}}^B(t = k_f; \Delta\omega) = \gamma_B^2 \frac{|\psi_{k_f,j}^B|^4}{(\Delta\omega - \varepsilon_{k_f,j})^2 + \gamma^2}, \quad (7)$$

with $\varepsilon_{k_f,j}$ and $\psi_{k_f,j}^B$ being determined by Eqs. (4)-(5). Previous works have demonstrated that the photonic band structure can be measured by time-resolved transmission spectroscopy, where the drop-port output transmission signal is obtained by scanning the frequency of the input laser linearly with time^{23,25}. Therefore, Eq. (7) indicates that the band structures read out from the drop-port output of ring B exhibit the projection of the band structure on the mode B_k in k_f space.

On the other hand, for the case of A *in*→A *out* by changing the input/output port to ring A, similar input/output coupled amplitude equations can be obtained. The amplitude of the output field at the drop port in the ring A is described by $S_{\text{out}}^A = -i\sqrt{\gamma_A} \sum_n [v_{a,n} e^{-i\omega_n t} + v_{c,n} e^{-i(\omega_n + \Omega/2)t}]$, with γ_A being the waveguide-resonator coupling strength of ring A. The corresponding normalized drop-port transmissions in the k_f space are [see supplementary materials]

$$T_{\text{out}}^A(t = k_f; \Delta\omega) = \gamma_A^2 \frac{|\psi_{k_f,j}^A|^2 |\psi_{k_f,j}^A + \psi_{k_f,j}^C|^2}{(\Delta\omega - \varepsilon_{k_f,j})^2 + \gamma^2}, \quad (8)$$

$$T_{\text{out}}^A(t = k_f; \Delta\omega + \Omega/2) = \gamma_A^2 \frac{|\psi_{k_f,j}^C|^2 |\psi_{k_f,j}^A + \psi_{k_f,j}^C|^2}{(\Delta\omega - \varepsilon_{k_f,j})^2 + \gamma^2}, \quad (9)$$

where Eq. (8) and Eq. (9) refer to the situation of an input field near resonant with the reference frequency ω_0 and $\omega_0 + \Omega/2$, respectively. This means that the band structure resolved from the drop-port transmission through the ring A is the projection of the band structure on the modes A_k and C_k separated by $\Omega/2$

along the frequency dimension.

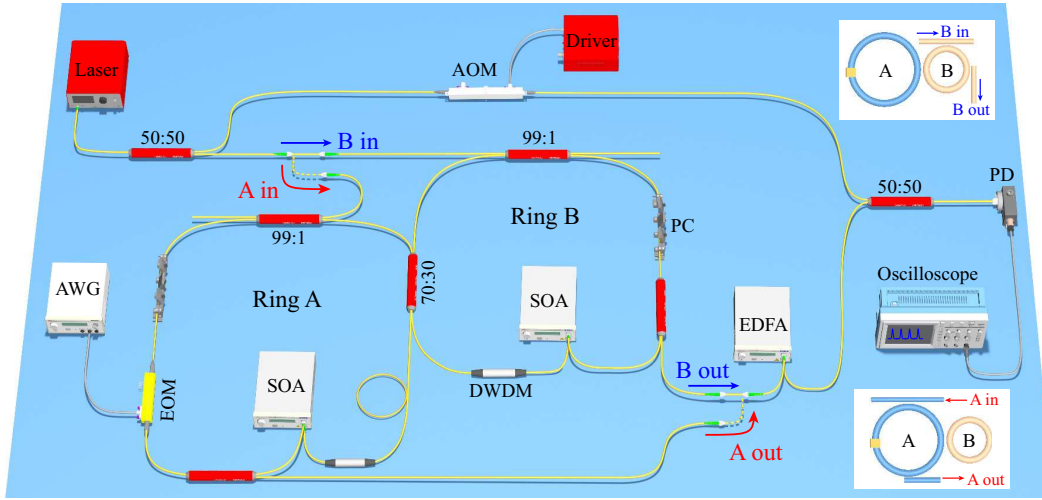


Figure 2. Experimental setup. EOM: electro-optic phase modulator. AOM: acousto-optic modulation. SOA: semiconductor optical amplifier. AWG: arbitrary waveform generator. EDFA: erbium-doped optical fiber amplifier. PC: polarization controller. DWDM: dense wavelength division multiplexing. PD: photodiode. Inserted: sketches of $B \text{ in} \rightarrow B \text{ out}$ and $A \text{ in} \rightarrow A \text{ out}$.

Different from previous experiments conducted in a single ring, the construction of the synthetic Lieb lattice requires two coupled rings, which faces the challenge of fully synchronizing resonant modes in two rings while one ring is undergoing dynamic modulation. In experiments, we use two fiber ring resonators coupled together through a 2×2 fiber coupler with coupler ratio 70:30 as shown in Fig. 2 (see Methods). The two rings are excited separately by selectively choosing ring A or ring B as the input port of the laser source ($A \text{ in}$ or $B \text{ in}$), while the transmission is recorded from the corresponding drop port ($A \text{ out}$ or $B \text{ out}$). After calibration, the lengths of the two rings are $L_A = 20.4 \text{ m}$ and $L_B = 10.2 \text{ m}$, corresponding to $\Omega_A = 2\pi \cdot 10 \text{ MHz}$ and $\Omega_B = 2\pi \cdot 20 \text{ MHz}$. To form the synthetic Lieb lattice described in Fig. 1(b), we drive the EOM in ring A by a sinusoidal radio frequency (RF) signal in the form of $V_M \cos(\Omega_M t + \phi)$ with $\Omega_M = 2\pi \cdot 10 \text{ MHz}$, and $\phi = -0.5\pi$.

To demonstrate the construction of the synthetic photonic Lieb lattice in the experiment, we perform the band structure measurements by finely sweeping the frequency of the input laser through multiple free-spectral ranges²⁵. We first inject the laser source into the input port of ring B and measure the output transmission spectra from the drop port of ring B ($B \text{ in} \rightarrow B \text{ out}$). Figure 3(a1)-(d1) plot the time-resolved band structures with varying modulation amplitude V_M , which are obtained by breaking the measured output transmission signals in Figs. 3(a3)-(d3) into time slices with the time window equaling

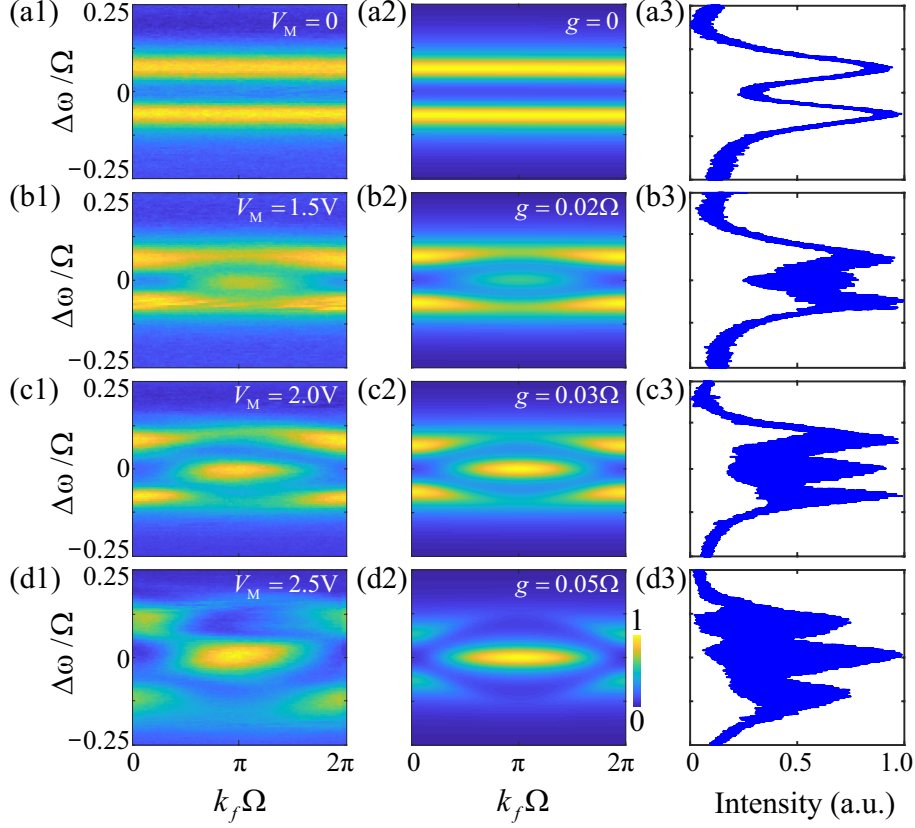


Figure 3. Band structure measurements for the case of B $in \rightarrow$ B out . (a1)-(d1) Experimentally observed band structures with different modulation amplitudes V_M . (a2)-(d2) Simulation results of the projected output intensity distribution of the band structure on mode B_k , based on Eqs. (4)-(5) and (7), where g takes different values with fixed $\kappa = 0.06\Omega$ and $\phi = -0.5\pi$. (a3)-(d3) Measured transmission spectra from the drop port of ring B. The vertical axis represents the frequency detuning of the input laser source normalized to Ω , while the bottom horizontal axis in (a1)-(d2) represents one roundtrip time in ring B with the period of $2\pi/\Omega$.

to one roundtrip time of ring B ($2\pi/\Omega$), i.e., the periodicity of the synthetic Lieb lattice. We calculate the intensity projections of the band structure on the mode B_k using Eq. (7) and show the results in Figs. 3(a2)-(d2). Without modulation ($V_M = 0$), one sees that coupled rings result in two Lorentzian resonances of the unmodulated rings which are slightly overlapped due to the lineshape broadening from the loss of the system [see Fig. 3(a3)]. It leads to two straight energy bands with constant intensity distributions in both experiment [see Fig. 3(a1)] and theory [see Fig. 3(a2)]. The feature of synthetic Lieb lattice begins to manifest once the modulation is applied as shown in Figs. 3(b1)-(d1), where one notices that there exists three bands and the intensity distributions vary with the modulation amplitude. For a small modulation amplitude [see Fig. 3(b1) with $V_M = 1.5$ V], the energy of the eigenstate mainly focuses on the upper and

lower dispersive bands, which transfers to the middle flat band when the modulation strength becomes larger as shown in Fig. 3(d1) with $V_M = 2.5$ V. The theoretical plots exhibit excellent agreement with experimental measurements, which clearly shows that the energy of the eigenstate flows from dispersive bands to the flat band when increasing g [see Fig. 3(b2)-(d2)]. Moreover, the intensity distributions on the two dispersive bands have symmetric pattern within the first Brillouin zone of $k_f \in [0, 2\pi/\Omega]$, which is consistent to the analytical solutions in Eq. (5).

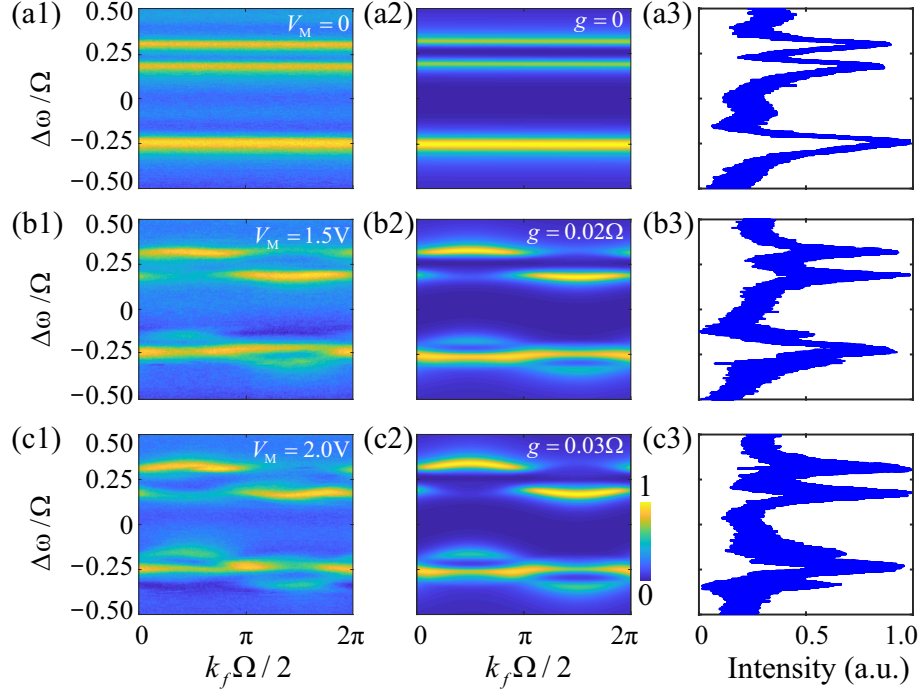


Figure 4. Band structure measurements for the case of A $in \rightarrow$ A out . (a1)-(c1) Experimentally observed band structures varied with V_M . (a2)-(c2) Simulation results of the projected intensity distribution of the band structure on modes A_k and C_k , based on Eqs. (4)-(5) and (8)-(9), with $\kappa = 0.06\Omega$ and $\phi = -0.5\pi$. (a3)-(c3) Transmission spectra measured from the drop port of ring A. The bottom horizontal axis in (a1)-(c2) represents one roundtrip time in ring A with the period of $4\pi/\Omega$.

We then consider the case of A $in \rightarrow$ A out by switching the input and output fiber to ring A. The output transmissions of modes A_k and C_k separated by $\Omega/2$ are measured simultaneously as shown in Figs. 4(a3)-(c3). Since in experiments, the time window to break the measured output transmission signals of ring A equals to one roundtrip time of ring A ($4\pi/\Omega$), we measure a combination of intensity projections of the band structure on A_k and C_k , which gives $k_f \in [0, 4\pi/\Omega]$ as plotted in Figs. 4(a1)-(c1). Theoretical results from Eqs. (8)-(9) are plotted in Figs. 4(a2)-(c2). When there is no modulation, one

sees two nearby straight bands near $\Delta\omega/\Omega = 0.25$ due to the energy splitting from coupling between modes A_n and B_n , and one single straight band near $\Delta\omega/\Omega = -0.25$ referring to the resonance of C_n in both experiment and theory [see Fig. 4(a1)-(a2)]. When the modulation is applied, the band structures near $\Delta\omega/\Omega = \pm 0.25$ show different features. For upper bands near $\Delta\omega/\Omega = 0.25$, one sees two dispersive bands, corresponding to the band structure in Fig. 1(c) projected to modes A_k [see Fig. 4(b1)-(c1)], which matches well with the calculated results by the formula in Eq. (8) [see Fig. 4(b2)-(c2)]. On the other hand, for lower bands near $\Delta\omega/\Omega = -0.25$, one can clearly see three bands, with the middle one being flat. The intensity projections of two dispersive bands on mode C_k are relatively weak in both experiment and theory. Both the intensity distributions of the two dispersive bands on the mode A_k and C_k have the asymmetric patterns within one period, which matches with the theoretical result in Eq. (5). We shall emphasize that the periodicity of the signal with a time window being $4\pi/\Omega$ can also be noticed from the term $|\psi_{k_f,j}^A + \psi_{k_f,j}^C|^2$, which is a unique characteristics from our system that signal amplitudes from modes A_n and C_n are mixed in the experiment. Furthermore, the roughness of transmission spectra in both Figs. 3 and 4 originates from the small display of frequency detuning range for containing multiple sinusoidal signal periods²⁵.

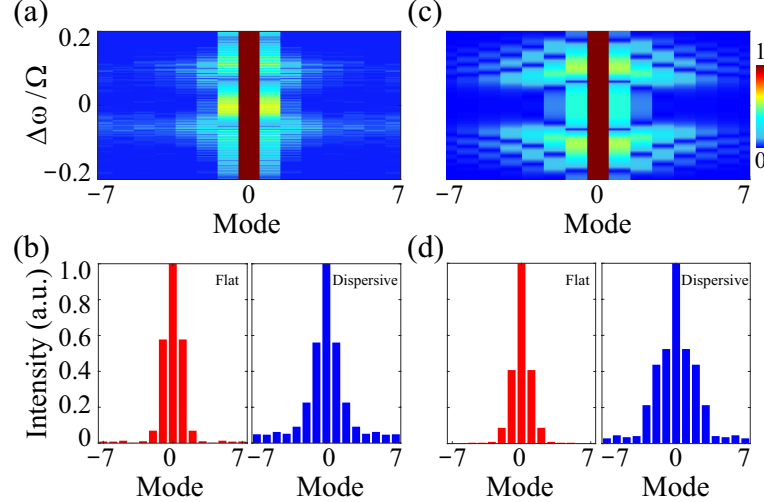


Figure 5. Mode distributions for the case of B in \rightarrow B out. (a) Experimentally resolved resonant mode spectra as a function of frequency detuning with $V_M = 3$ V. (b) The corresponding mode distributions of two selected input frequencies in (a) located at $\Delta\omega = 0$ and $\Delta\omega = 0.08\Omega$, respectively. (c) Simulated resonant mode spectra $|v_{b,n}|^2$ with $g = \kappa = 0.06\Omega$, and (d) the corresponding intensity distributions of the two chosen input frequencies at $\Delta\omega = 0$ and $\Delta\omega = 0.08\Omega$, respectively. The horizontal axis represents the mode number n for the frequency ω_n .

Next, we measure the frequency mode distributions for the case of B in \rightarrow B out by the heterodyne

detection method to probe the localization effect of flat band in the synthetic Lieb lattice. We connect the AOM path in Fig. 2 for frequency shift, and interfere it with the drop-port output of ring B by a 50:50 fiber coupler. To show evolutions of frequency modes through out the whole band structure, we sweep the input laser frequency near the resonance frequency ω_0 , and process the drop-port output transmission through the fast Fourier transform⁴³. Figure 5(a) shows the experimentally resolved mode distributions as a function of frequency detuning $\Delta\omega$, where the intensities of modes are well confined near $\Delta\omega \sim 0$, which refers to the flat band, but spreads over the dispersive bands at $\Delta\omega \sim \pm 0.07\Omega$. We explicitly exhibit the mode intensity distributions for two input frequencies in Fig. 5(b), which are $\Delta\omega = 0$ at the flat band and $\Delta\omega = 0.08\Omega$ at the upper dispersive band, respectively. For the input frequency at the flat band [see the left part of Fig. 5(b)], one sees that the intensities of modes B_n mainly locate at the 0th and $\pm 1^{\text{st}}$ modes with very small portion diverging to the $\pm 2^{\text{nd}}$ modes. On the other hand, intensities of modes experience spread for the input frequency located at the dispersive band [see the right part of Fig. 5(b)]. Simulations are performed by solving Eq. (7) with sweeping the input frequency and then Fourier transforming the transmitted signal. One can see a good agreement between experimental measurement in Figs. 5(a)-(b) and simulated results in Figs. 5(c)-(d).

One notes that the existence of the flat band in the constructed synthetic Lieb lattice is not dependent on the coupling coefficients, i.e., g and κ for the weak modulation condition³⁴. Further increase of the modulation strength falls on the break of the synthetic Lieb lattice under the tight-binding limit. In this structure, one can make the band transition between the flat band and non-flat band by simply adding the higher-order modulation to introduce the long-range couplings in the frequency dimension, i.e., with an additional modulation frequency Ω , which makes the modulation being $2g \cos(\Omega t/2 + \phi) + 2g' \cos(\Omega t + \phi')$. The second term in the modulation brings next-nearest-neighbor couplings between two nearby resonant modes A_n (or C_n). In experiment, we apply the EOM in ring A with the corresponding form of $V_M \cos(\Omega_M t + \phi) + V'_M \cos(2\Omega_M t + \phi')$ where $\Omega_M = 2\pi \cdot 10$ MHz, and $\phi = \phi' = -0.5\pi$, and perform the measurements in the case of B *in*→B *out*, which are shown in Fig. 6. Without higher-order modulation [see Fig. 6(a1) with $V'_M = 0$], the system exhibits the feature of flat band, which is the same with Figs. 3(c1)-(c2). Once the higher-order modulation term is added into EOM ($V'_M \neq 0$), the middle band gradually turns into dispersive, while the upper and lower dispersive bands start to show the nonsymmetric feature as shown in Figs. 6(b1)-(d1). In addition, the gap throughout the entire k_f space gets closed if V'_M becomes larger [see Fig. 6(d1)]. We therefore show the transition from flat to non-flat bands in Figs. 6(a1)-(d1), which are excellently agreed with the simulations results in Figs. 6(a2)-(d2).

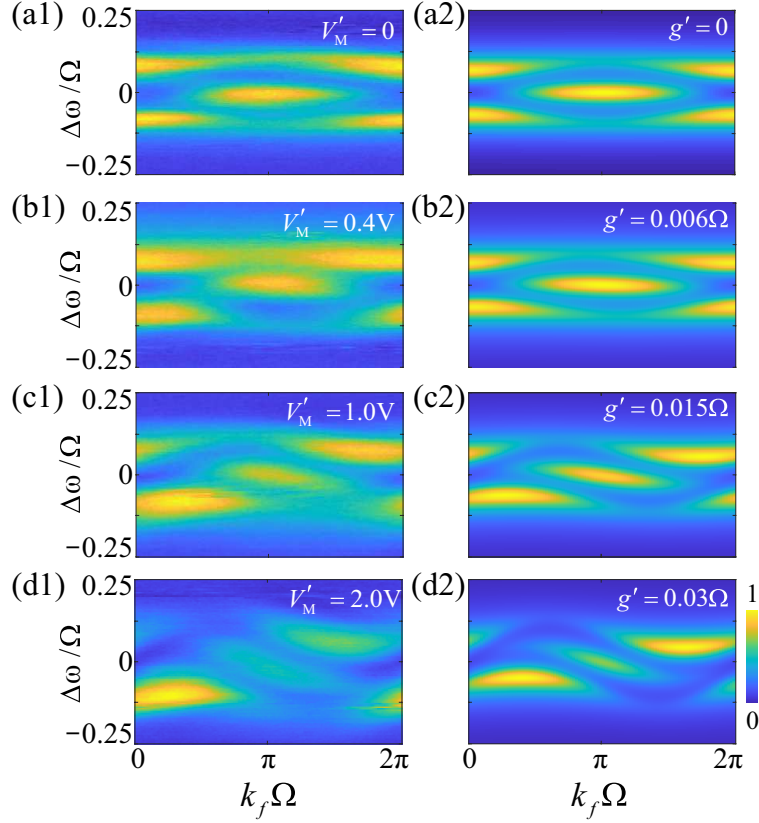


Figure 6. Observations of flat to non-flat band transition for the case of $B_{in} \rightarrow B_{out}$. (a1)-(d1)

Experimentally measured band structures with different long-range modulation amplitudes V'_M and fixed $V_M = 2$ V. (a2)-(d2) Simulation results of the projected intensity distribution of the band structure on mode B_k varied with g' , where $g = 0.03\Omega$ and $\phi = \phi' = -0.5\pi$.

Such opportunity to dynamically introduce the band transition could be useful for light stopping, which has been proposed in theory^{44,45}.

Our construction of the Lieb lattice in two coupled rings, which is more complex than the 1D lattice in the frequency dimension in a single modulated ring^{23–25,27–30}, proves the experimental feasibility in connecting multiple rings with different types while simultaneously constructing synthetic frequency dimension. Our experiments also points to important future opportunities for experimentally implementing other complicated synthetic lattice structures in multiple rings, such as square lattice²¹, honeycomb lattice⁷, and lattice supporting high-order topology^{46,47}, which have been intensively studied in theory⁴. Moreover, miniaturization of modulated rings is also possible thanks to the advances of integrated on-chip platforms^{27,30}.

In summary, we have experimentally demonstrated a 1D synthetic photonic Lieb lattice along the

frequency axis of light, constructed by two coupled fiber ring resonators at different types. Flat band gapped from two dispersive bands are observed under both two cases by selectively choosing the input and output ports for excitations and transmission measurements, which shows that measured band structures are intensity projections of the band on the different resonant modes in k_f space. We also observe localization effect near the flat band with distinctive feature from dispersive bands, and demonstrate the flat to non-flat band transition by adding the long-range couplings in modulations, characterizing the intrinsic physics of the synthetic Lieb lattice. Theoretical simulations are performed and agree well with experimental results, which shows unique feature of synthetic frequency dimension in measurements where signal from two modes are combined. Our work opens a door for experimentally constructing more complicated photonic lattice with the synthetic frequency dimension, showing important promise for optical communications in fiber-based or on-chip resonators⁴⁸, and also highlighting potentials towards non-Hermitian/topological^{49–53} and quantum photonics^{54–57} in coupled modulated ring resonator systems.

Methods

Experimental setup. The frequency of the laser source can be finely tuned over 30 GHz by applying an external ramp signal to its frequency modulation input, with the central wavelength located at 1550.92 nm. Near 50% of the laser source is sent to an acousto-optic modulation (AOM) for frequency shift and heterodyne beating with the drop-port output^{58,59}. In each ring, a 2×2 fiber coupler couples 1% of the remaining 50% laser source to the ring resonator, after which a polarization controller is used to adjust the polarization of laser circulating in the ring. To achieve a high quality factor for the resonator, a semiconductor optical amplifier (SOA) is used to compensate the loss in the ring with a maximum gain of 10 dB. A dense wavelength division multiplexing with a central wavelength of 1550.92 nm (international telecommunication union channel 33) is used to filter the amplified emission noise from SOA. Ring A undergoes dynamic modulation by a lithium niobate EOM with a 10 GHz bandwidth, which is driven by an arbitrary waveform generator with 200 MHz bandwidth. A 1×2 fiber coupler couples 0.5% of the signal out of the ring, which is then amplified by an erbium-doped optical fiber amplifier (with maximum gain of 12 dB) to boost the signal-to-noise ratio before it gets detected by a fast InGaAs photodiode (850 to 1650 nm with 10 GHz bandwidth) and sent to the oscilloscope (5 Gsamples/s with 1 GHz bandwidth). For the flat band structure measurement (Figs. 3 and 4), we disconnect the AOM path, and only connect it for the resonant mode observation (Fig. 5). In addition, we also place an EOM in ring B just for

calibrating the length of ring B, which is not shown in Fig. 2.

The lengths of the two rings need accurate calibration for stabilize the connectivity between the resonant modes to construct the synthetic Lieb lattice. We first separately measure the FSRs of ring A and ring B by disconnecting the 70:30 fiber coupler. For each ring, we vary the modulation frequency by linearly sweeping the input frequency until the modulation sidebands fully overlap with the resonant modes. We then adjust fiber's length to make up for the required FSR difference. One can also place an optical delay in the ring to finely tuning the length. Noting that the fiber coupler used to couple the two rings together in Fig. 2 keeps 70% of the light power remained in the excited ring and the left 30% coupled to the other ring no matter which ring we choose to excite, which gives the same coupling strengths for both cases.

Data availability

Source data are provided with this paper. All other data that support the plots within this paper and other findings of this study are available from the corresponding authors upon reasonable request.

Acknowledgements

We greatly thank Prof. Shanhui Fan for fruitful discussions. The research is supported by National Natural Science Foundation of China (12122407, 11974245, and 12104297), National Key R&D Program of China (2017YFA0303701), Shanghai Municipal Science and Technology Major Project (2019SHZDZX01), Natural Science Foundation of Shanghai (19ZR1475700), and China Postdoctoral Science Foundation (2020M671090). L.Y. acknowledges support from the Program for Professor of Special Appointment (Eastern Scholar) at Shanghai Institutions of Higher Learning. X. C. also acknowledges the support from Shandong Quancheng Scholarship (00242019024).

Author contributions

G.L. conceived the idea with L.Y. and X.C., and designed the experiment. G.L., L.W. and L.Y. developed the theoretical analysis and simulations. G.L. and R.Y. carried out the experiment with assistance from S.L. and Y.Z. L.Y. and X.C. revised the manuscript. All authors contributed to discussion of the results and preparation of the manuscript. G.L., L.Y. and X.C. supervised the project.

Competing interests

The authors declare no competing interests.

References

1. Yuan, L., Lin, Q., Xiao, M. & Fan, S. Synthetic dimension in photonics. *Optica* **5**, 1396–1405 (2018).
2. Ozawa, T. & Price, H. M. Topological quantum matter in synthetic dimensions. *Nat. Rev. Phys.* **1**, 349–357 (2019).
3. Lustig, E. & Segev, M. Topological photonics in synthetic dimensions. *Adv. Opt. Photon.* **13**, 426–461 (2021).
4. Yuan, L., Dutt, A. & Fan, S. Synthetic frequency dimensions in dynamically modulated ring resonators. *APL Photonics* **6**, 071102 (2021).
5. Schwartz, A. & Fischer, B. Laser mode hyper-combs. *Opt. Express* **21**, 6196–6204 (2013).
6. Qin, C. *et al.* Spectrum control through discrete frequency diffraction in the presence of photonic gauge potentials. *Phys. Rev. Lett.* **120**, 133901 (2018).
7. Yuan, L., Xiao, M., Lin, Q. & Fan, S. Synthetic space with arbitrary dimensions in a few rings undergoing dynamic modulation. *Phys. Rev. B* **97**, 104105 (2018).
8. Lustig, E. *et al.* Photonic topological insulator in synthetic dimensions. *Nature* **567**, 356–360 (2019).
9. Wang, K. *et al.* Multidimensional synthetic chiral-tube lattices via nonlinear frequency conversion. *Light. Sci. Appl.* **9**, 1–10 (2020).
10. Regensburger, A. *et al.* Photon propagation in a discrete fiber network: An interplay of coherence and losses. *Phys. Rev. Lett.* **107**, 233902 (2011).
11. Regensburger, A. *et al.* Parity-time synthetic photonic lattices. *Nature* **488**, 167–171 (2012).
12. Luo, X. *et al.* Quantum simulation of 2D topological physics in a 1D array of optical cavities. *Nat. Commun.* **6**, 7704 (2015).
13. Bell, B. A. *et al.* Spectral photonic lattices with complex long-range coupling. *Optica* **4**, 1433–1436 (2017).

14. Ozawa, T. & Carusotto, I. Synthetic dimensions with magnetic fields and local interactions in photonic lattices. *Phys. Rev. Lett.* **118**, 013601 (2017).
15. Peterson, C. W., Benalcazar, W. A., Lin, M., Hughes, T. L. & Bahl, G. Strong nonreciprocity in modulated resonator chains through synthetic electric and magnetic fields. *Phys. Rev. Lett.* **123**, 063901 (2019).
16. Yuan, L. *et al.* Photonic gauge potential in one cavity with synthetic frequency and orbital angular momentum dimensions. *Phys. Rev. Lett.* **122**, 083903 (2019).
17. Cheng, D. *et al.* Arbitrary synthetic dimensions via multiboson dynamics on a one-dimensional lattice. *Phys. Rev. Res.* **3**, 033069 (2021).
18. Jukić, D. & Buljan, H. Four-dimensional photonic lattices and discrete tesseract solitons. *Phys. Rev. A* **87**, 013814 (2013).
19. Petrides, I., Price, H. M. & Zilberberg, O. Six-dimensional quantum Hall effect and three-dimensional topological pumps. *Phys. Rev. B* **98**, 125431 (2018).
20. Zilberberg, O. *et al.* Photonic topological boundary pumping as a probe of 4D quantum Hall physics. *Nature* **553**, 59–62 (2018).
21. Yuan, L., Shi, Y. & Fan, S. Photonic gauge potential in a system with a synthetic frequency dimension. *Opt. Lett.* **41**, 741–744 (2016).
22. Ozawa, T., Price, H. M., Goldman, N., Zilberberg, O. & Carusotto, I. Synthetic dimensions in integrated photonics: From optical isolation to four-dimensional quantum Hall physics. *Phys. Rev. A* **93**, 043827 (2016).
23. Dutt, A. *et al.* Experimental band structure spectroscopy along a synthetic dimension. *Nat. Commun.* **10**, 3122 (2019).
24. Dutt, A. *et al.* A single photonic cavity with two independent physical synthetic dimensions. *Science* **367**, 59–64 (2020).
25. Li, G. *et al.* Dynamic band structure measurement in the synthetic space. *Sci. Adv.* **7**, eabe4335 (2021).
26. Weidemann, S. *et al.* Topological funneling of light. *Science* **368**, 311–314 (2020).

27. Hu, Y., Reimer, C., Shams-Ansari, A., Zhang, M. & Loncar, M. Realization of high-dimensional frequency crystals in electro-optic microcombs. *Optica* **7**, 1189–1194 (2020).
28. Chen, H. *et al.* Real-time observation of frequency Bloch oscillations with fibre loop modulation. *Light. Sci. Appl.* **10**, 1–9 (2021).
29. Wang, K. *et al.* Generating arbitrary topological windings of a non-Hermitian band. *Science* **371**, 1240–1245 (2021).
30. Balčytis, A. *et al.* Synthetic dimension band structures on a Si CMOS photonic platform. *arXiv:2105.13742* (2021).
31. Lin, Q., Sun, X.-Q., Xiao, M., Zhang, S.-C. & Fan, S. A three-dimensional photonic topological insulator using a two-dimensional ring resonator lattice with a synthetic frequency dimension. *Sci. Adv.* **4**, eaat2774 (2018).
32. Wang, K., Dutt, A., C. Wojcik, C. & Fan, S. Topological complex-energy braiding of non-hermitian bands. *Nature*, accepted (2021).
33. Mukherjee, S. *et al.* Observation of a localized flat-band state in a photonic Lieb lattice. *Phys. Rev. Lett.* **114**, 245504 (2015).
34. Baboux, F. *et al.* Bosonic condensation and disorder-induced localization in a flat band. *Phys. Rev. Lett.* **116**, 066402 (2016).
35. Leykam, D., Andreanov, A. & Flach, S. Artificial flat band systems: from lattice models to experiments. *Adv. Phys. : X* **3**, 1473052 (2018).
36. Xia, S. *et al.* Unconventional flatband line states in photonic Lieb lattices. *Phys. Rev. Lett.* **121**, 263902 (2018).
37. Ma, J. *et al.* Direct observation of flatband loop states arising from nontrivial real-space topology. *Phys. Rev. Lett.* **124**, 183901 (2020).
38. Yu, D., Yuan, L. & Chen, X. Isolated photonic flatband with the effective magnetic flux in a synthetic space including the frequency dimension. *Laser Photon. Rev.* **14**, 2000041 (2020).
39. Scully, M. O. & Zubairy, M. S. *Quantum Optics* (Cambridge University Press, 1997).
40. Hyrkäs, M., Apaja, V. & Manninen, M. Many-particle dynamics of bosons and fermions in quasi-one-dimensional flat-band lattices. *Phys. Rev. A* **87**, 023614 (2013).

41. Rojas-Rojas, S., Morales-Inostroza, L., Vicencio, R. A. & Delgado, A. Quantum localized states in photonic flat-band lattices. *Phys. Rev. A* **96**, 043803 (2017).
42. Huda, M. N., Kezilebieke, S. & Liljeroth, P. Designer flat bands in quasi-one-dimensional atomic lattices. *Phys. Rev. Res.* **2**, 043426 (2020).
43. Nussbaumer, H. J. The fast Fourier transform. In *Fast Fourier Transform and Convolution Algorithms*, 80–111 (Springer, 1981).
44. Yanik, M. F. & Fan, S. Stopping light all optically. *Phys. Rev. Lett.* **92**, 083901 (2004).
45. Sandhu, S., Povinelli, M. L., Yanik, M. F. & Fan, S. Dynamically tuned coupled-resonator delay lines can be nearly dispersion free. *Opt. Lett.* **31**, 1985–1987 (2006).
46. Zhang, W. & Zhang, X. Quadrupole topological phases in the zero-dimensional optical cavity. *Eur. Lett.* **131**, 24004 (2020).
47. Dutt, A., Minkov, M., Williamson, I. A. D. & Fan, S. Higher-order topological insulators in synthetic dimensions. *Light. Sci. Appl.* **9**, 1–9 (2020).
48. Chen, Z. & Segev, M. Highlighting photonics: looking into the next decade. *eLight* **1**, 1–12 (2021).
49. Peng, B. *et al.* Parity-time-symmetric whispering-gallery microcavities. *Nat. Phys.* **10**, 394–398 (2014).
50. Wimmer, M. *et al.* Observation of optical solitons in PT-symmetric lattices. *Nat. Commun.* **6**, 7782 (2015).
51. Ozawa, T. *et al.* Topological photonics. *Rev. Mod. Phys.* **91**, 015006 (2019).
52. Song, Y. *et al.* Two-dimensional non-Hermitian skin effect in a synthetic photonic lattice. *Phys. Rev. Appl.* **14**, 064076 (2020).
53. Guo, Q. *et al.* Experimental observation of non-Abelian topological charges and edge states. *Nature* **594**, 195–200 (2021).
54. Boutari, J. *et al.* Large scale quantum walks by means of optical fiber cavities. *J. Opt.* **18**, 094007 (2016).
55. Chen, C. *et al.* Observation of topologically protected edge states in a photonic two-dimensional quantum walk. *Phys. Rev. Lett.* **121**, 100502 (2018).

56. Chalabi, H. *et al.* Synthetic gauge field for two-dimensional time-multiplexed quantum random walks. *Phys. Rev. Lett.* **123**, 150503 (2019).
57. Joshi, C. *et al.* Frequency-domain quantum interference with correlated photons from an integrated microresonator. *Phys. Rev. Lett.* **124**, 143601 (2020).
58. Wildi, T., Voumard, T., Brasch, V., Yilmaz, G. & Herr, T. Photo-acoustic dual-frequency comb spectroscopy. *Nat. Commun.* **11**, 4146 (2020).
59. Tetsumoto, T. *et al.* Optically referenced 300 GHz millimetre-wave oscillator. *Nat. Photonics* **15**, 516–522 (2021).